(Preprint) AAS 11-427

MULTI-BODY CAPTURE TO LOW-ALTITUDE CIRCULAR ORBITS AT EUROPA

Daniel J. Grebow,* Anastassios E. Petropoulos,* Paul A. Finlayson*

For capture to a 200-km circular orbit around Europa, millions of different points along the orbit are simulated in the Jupiter-Europa Restricted 3-Body Problem. The transfers exist as members of families of trajectories, where certain families consistently outperform the others. The trajectories are not sensitive to changes in inclination for the final circular orbit. The top performing trajectories appear to follow the invariant manifolds of L_2 Lyapunov orbits for capture into a retrograde orbit, and in some cases saving up to 40% of the Δv from the patched 2-body problem. Transfers are attached to the current nominal mission for NASA's Jupiter-Europa Orbiter, where the total cost is roughly 100 m/s less than the baseline mission.

INTRODUCTION

NASA engineers and scientists have long anticipated a mission to Europa. While a mission to Europa is enticing for many reasons, the primary cause of our allurement is the potential discovery of "habitable worlds".[1] Scientists speculate that buried beneath the surface of this moon is a water ocean that might support life.

There are many options for a mission to Europa.[2,3,4,5] The currently proposed mission architecture consists of two spacecraft: the NASA-led Jupiter-Europa Orbiter (JEO) and the ESA-led Jupiter-Ganymede Orbiter (JGO). The nominal trajectory for JEO would involve many phases, including multiple interplanetary flybys and over 20 flybys of the Jovian moons.[5] Nearing the end of its three-year campaign, eventually the spacecraft would fall into a cadence, or resonance, with Europa's orbit. This phase would be just the beginning of what researchers have dubbed *endgame*;[3] however, considering the dance the spacecraft plays with Europa at this time, a more adequate description might be *courtship*. For a final play, the spacecraft would capture into a 200-km circular orbit around Europa. As far as the scientists are concerned, the end of this phase marks the beginning of what would hopefully be a long list of discoveries at Europa.

Ignoring Earth launch and Jupiter orbit insertion, Kloster et al.[5] report that the entire tour would require less than 1 km/s in deterministic Δv. Since the bulk of this Δv is at Europa orbit insertion (EOI), the primary motivation for the current work is to develop a practical technique for designing an efficient capture at Europa. Efficient capture means harnessing the gravitational effects of both Europa and Jupiter to lower the insertion cost. This is primarily a three-body problem, and therefore inherits all the features associated with the three-body problem, i.e., numerical integration in highly sensitive regimes. Of course, the radiation dose is also a concern, and therefore a technique cannot lead to unrealistically long trajectories that spend too much time in the radiation belts.

In the literature, there are only a few studies on efficient capture to low altitude orbits at Europa. Koon et al.[6] utilize the invariant manifolds of periodic orbits for designing a ballistic capture. While this approach is appealing from a dynamical systems perspective, the final orbit for JEO would be at an altitude from which ballistic capture is impossible. Still the method might be adapted for designing capture trajectories with low insertion costs. Campagnola and Russell[7] mainly focus on methods for minimizing the apoapsis Δv's leading

*Mission Design Engineer, Outer Planet Mission Analysis, Jet Propulsion Laboratory, California Institute of Technology, 4800 Oak Grove, Pasadena, CA, 91109-8099.

up to EOI, however, in another study[8] they include a multi-body approach that might be useful for unlocking efficient capture trajectories. Starting from a 100-km circular orbit around Europa, they numerically integrate trajectories backwards in the Jupiter-Europa Restricted 3-Body Problem (R3BP). Sampling various departure geometries, they are able to find a transfer originating from Ganymede that captures with only $\Delta v = 0.51$ km/s, well below the minimum Δv for parabolic capture in the Patched 2-Body Problem (P2BP). Unfortunately, their method is tied to a very specific mission objective (i.e., transfer from a 100-km Ganymede orbit), and it is difficult to see how to adapt their approach for a general baseline mission strategy. Furthermore, they only investigate a planar circular orbit at Europa, and the mission requirements stipulate that the orbit must be inclined at $95°$ to the equator.

Johannesen and D'Amario[3] discuss multiple options for the Jovian tour, each ending with only 520 m/s for EOI. Since their analysis is more focused on mission architectures, they do not provide a detailed description of the method used to generate the trajectories. In fact, the algorithm was written by one of the authors (Finlayson) on this current paper, and, in brief, goes as follows: A database of stored trajectories are calculated by starting from a 200-km circular orbit around Europa and numerically integrating three-body equations backwards to the first apojove. The precise initial conditions for integration are obtained by applying a maneuver tangent to the spacecraft's velocity vector for all possible geometries of an orbit at a prescribed inclination. Only the trajectories that yield the highest apojoves are stored. While considering phasing between the spacecraft, Jupiter, and Europa, the final Europa flyby is adjusted until a trajectory matches in position with one of the stored trajectories.

The current work expounds upon the method used by Johannesen and D'Amario to arrive at a more satisfying dynamical understanding of the solutions. Starting with a 200-km circular orbit around Europa, we also apply maneuvers tangent to the spacecraft's velocity vector. Recognizing the sensitivity of the dynamics, a million different locations along the orbit are sampled. Prograde and retrograde orbits are investigated, as well as when the orbit is inclined at $95°$ to Europa's orbital plane. The states for the points are simulated in backwards time in the Jupiter-Europa R3BP, where the final apojove values are recorded. After repeating the process for various EOI Δv's, we notice that each transfer trajectory exists as a member of a family of trajectories, where certain families consistently outperform others. The most desirable family appears to arrive along the invariant manifolds associated with an L_2 Lyapunov orbit. For some of the trajectories, the Δv savings is as high as 40% of the Δv computed in the P2BP. The study is completed with a method for patching the trajectories into the baseline mission for JEO.

SOLUTION APPROACH

Our goal is discovery of efficient capture trajectories that simultaneously leverage the gravitational effects of Jupiter and Europa. Therefore all capture simulations take place in the Jupiter-Europa R3BP. For a particular Δv, we seek to find the optimal insertion location to a 200-km circular orbit that originates from a trajectory with the highest possible apojove.

Equations of Motion

For the Jupiter-Europa R3BP,[9] the primary bodies are assumed to move in circular orbits, and the spacecraft possesses comparatively negligible mass. The standard rotating, barycentric coordinate frame is used, with the X-axis directed from Jupiter to Europa and the Z-axis parallel to the Jupiter-Europa angular velocity. The nondimensional form of the equations is

$$\begin{aligned}
\ddot{X} &= 2\dot{Y} + X + (\mu - 1)\frac{X + \mu}{d^3} - \mu\frac{X + \mu - 1}{r^3}, \\
\ddot{Y} &= -2\dot{X} + Y + (\mu - 1)\frac{Y}{d^3} - \mu\frac{Y}{r^3}, \\
\ddot{Z} &= (\mu - 1)\frac{Z}{d^3} - \mu\frac{Z}{r^3}.
\end{aligned} \tag{1}$$

where

$$\begin{aligned} d^2 &= (X+\mu)^2 + Y^2 + Z^2, \\ r^2 &= (X+\mu-1)^2 + Y^2 + Z^2. \end{aligned} \tag{2}$$

In Eq. (1), X, Y, and Z are the components of the spacecraft's position relative to the rotating, barycentric frame and μ is the mass parameter.

Methodology

Starting from a 200-km circular parking orbit around Europa, the approach is to apply a maneuver and integrate Eqs. (1) in backwards time. Since Europa is the dominant gravitating body when the spacecraft is in the 200-km circular orbit, we only consider maneuvers along the spacecraft's inertial velocity vector. The simulations are terminated at the first crossing of the plane $Y = 0$ where $X < 0$, and the osculating apojove is computed. When the trajectory crosses the plane $Y = 0$ where $X < 0$, the osculating apojove is very close to the actual apojove. The method is similar to the one used by Campagnola and Russell.[8]

To express the capture conditions as initial states for integrating Eq. (1), we first define the spacecraft's position and velocity in terms of polar coordinates centered at Europa. The position and velocity are

$$\mathbf{r} = (r_c, 0, 0)^T, \;\; \mathbf{v} = (0, \sqrt{\mu/r_c} + \Delta v, 0)^T, \tag{3}$$

where the quantity r_c is the nondimensional radius of the 200-km circular orbit, and recall μ is the Jupiter-Europa mass ratio. The transformation $\mathbf{T}$ from polar coordinates to an inertial frame instantaneously aligned with the Jupiter-Europa rotating frame is defined by an Euler 3-1-3 (Ω-i-θ) sequence, i.e.,

$$\mathbf{T} = \begin{bmatrix} \cos\Omega\cos\theta - \sin\Omega\sin\theta\cos i & -\cos\Omega\sin\theta - \sin\Omega\cos\theta\cos i & \sin\Omega\sin i \\ \sin\Omega\cos\theta + \cos\Omega\sin\theta\cos i & -\sin\Omega\sin\theta + \cos\Omega\cos\theta\cos i & -\cos\Omega\sin i \\ \sin\theta\sin i & \cos\theta\sin i & \cos i \end{bmatrix}, \tag{4}$$

where $0^\circ \leq i \leq 180^\circ$. Then, the position and velocity of the spacecraft in the barycentric rotating frame are

$$\begin{aligned} \mathbf{R} &= (X, Y, Z)^T = \mathbf{T}\mathbf{r} + (1-\mu, 0, 0)^T, \\ \mathbf{V} &= (\dot{X}, \dot{Y}, \dot{Z})^T = \mathbf{T}\mathbf{v} - (-Y, X+\mu-1, 0)^T. \end{aligned} \tag{5}$$

For circular orbits in the plane of the primaries, $\Omega = 0^\circ$. The orbit can be either pure prograde if $i = 0^\circ$ or pure retrograde when $i = 180^\circ$. For simplicity, hereafter, we refer to pure prograde and pure retrograde as *prograde* and *retrograde*, respectively. The quantities Δv, θ, Ω, and i encompass all possible capture trajectories. Furthermore, by Eq. (5), these parameters uniquely determine an initial state for integrating Eq. (1) in backwards time. In this study we allow Δv, θ, and Ω to vary for particular values of i.

Delta-v for L_2 Jacobi Constant

Jacobi's constant is a well-known integral of the motion in the R3BP, and has been useful in the past for understanding strategic placement of maneuvers.[10] In barycentric rotating coordinates, the integral is

$$C = -\dot{X}^2 - \dot{Y}^2 - \dot{Z}^2 + X^2 + Y^2 + 2(1-\mu)/d + 2\mu/r. \tag{6}$$

For trajectories entering the Jupiter-Europa system from ranges beyond Europa's orbit, the minimum possible Δv for insertion at Europa is the one that makes the Jacobi constant equal to that of L_2. At this Δv a small corridor, or gateway, opens at L_2 enabling low-energy transfer into the vicinity of Europa.[11] To compute this Δv, i.e., the Δv required to achieve C_{L_2}, we note that Eq. (6) can be expressed in terms of Δv, θ, Ω, and i using Eqs. (5). Setting $C = C_{L_2}$ and solving for Δv yields

$$\Delta v = r_c \cos i - \sqrt{\mu/r_c} + \sqrt{r_c^2 \cos^2\theta \sin^2 i + X^2 + Y^2 + 2(1-\mu)/d + 2\mu/r - C_{L_2}}. \tag{7}$$

For a particular value of i, we are interested in the smallest possible Δv for all values of θ and Ω. The global minimum is easily found by looping through θ and Ω and computing Δv with Eq. (7). As shown in Figure 1,

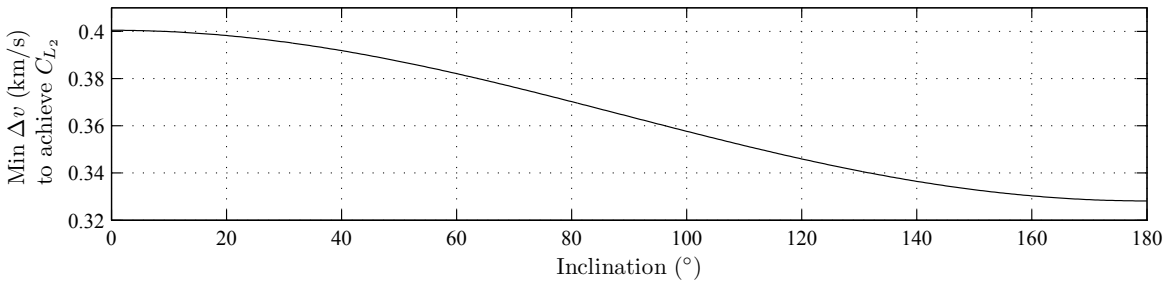

Figure 1. For 200-km circular Europa orbit, Δv necessary to achieve C_{L_2}.

the minimum Δv varies with inclination. The minimum Δv to achieve C_{L_2} for polar orbits is *less* than that required if the orbit is prograde. If the orbit is retrograde the Δv necessary is even smaller.

Here we arrive at an important results that is also noticed by Campagnola and Russell.[8] Europa's orbital motion imparts a rotational component of velocity on the spacecraft, reducing the cost for insertion into a retrograde orbit. From Eq. (7), the difference in cost for insertion into a prograde orbit ($\Delta v_{i=0^\circ}$) versus a retrograde orbit ($\Delta v_{i=180^\circ}$) is

$$\Delta v_{i=0^\circ} - \Delta v_{i=180^\circ} = 2r_c. \tag{8}$$

For a 200-km circular orbit, this difference is

$$\Delta v_{i=0^\circ} - \Delta v_{i=180^\circ} = 72.3 \text{ m/s}. \tag{9}$$

We note that the variation in cost for insertion to a prograde versus a retrograde orbit depends only on the radius of the orbit r_c, and is independent of the departure location θ well as the Jacobi constant resulting from applying the maneuver.

Passing through the L_2 corridor depends also on the phase space stability, so implementing a Δv that is slightly higher than those in Figure 1 does not guarantee that the spacecraft will ever pass through the gateway. However, the minimum Δv to achieve C_{L_2} is still useful in that it is the theoretical lower limit for capture in the R3BP, and is considerably less than $\Delta v = 558$ m/s, or the Δv for parabolic capture from the P2BP.

TRANSFERS TO IN-PLANE CIRCULAR ORBITS

The details of our approach are first outlined for transfers to prograde and retrograde orbits in Europa's orbital plane. We begin by sampling grid points along the capture trajectory. The grid search provides insight into various options for approaching Europa, and ultimately serves as a pool of initial guesses for an algorithm that further refines the trajectories.

Grid Search

Recall that for orbits in the plane of the primaries, $\Omega = 0^\circ$ and $i = 0^\circ$ or 180° depending on if the orbit is prograde or retrograde. Then, for a given Δv, the goal of a grid search is to determine the optimal EOI location θ. Due to the sensitivities in the R3BP, it is very difficult to predict a value of θ that maximizes the osculating apojove r_a. To search for these trajectories, we implement an extremely fine grid. For a given Δv, we examine 1 million capture trajectories where the initial state corresponds to 1 million linearly equally spaced points between $\theta = 0^\circ$ and 360°. As previously described, the trajectories are integrated to the first crossing of the plane $Y = 0$ where $X < 0$. All simulations are performed in Fortran 90 using Shampine and Watt's[12] Adams-Bashforth-Moulton variable time-stepping integrator. To investigate whether Δv cost actually decreases with integration time, we select a 500-day limit for all simulations so as not to exclude

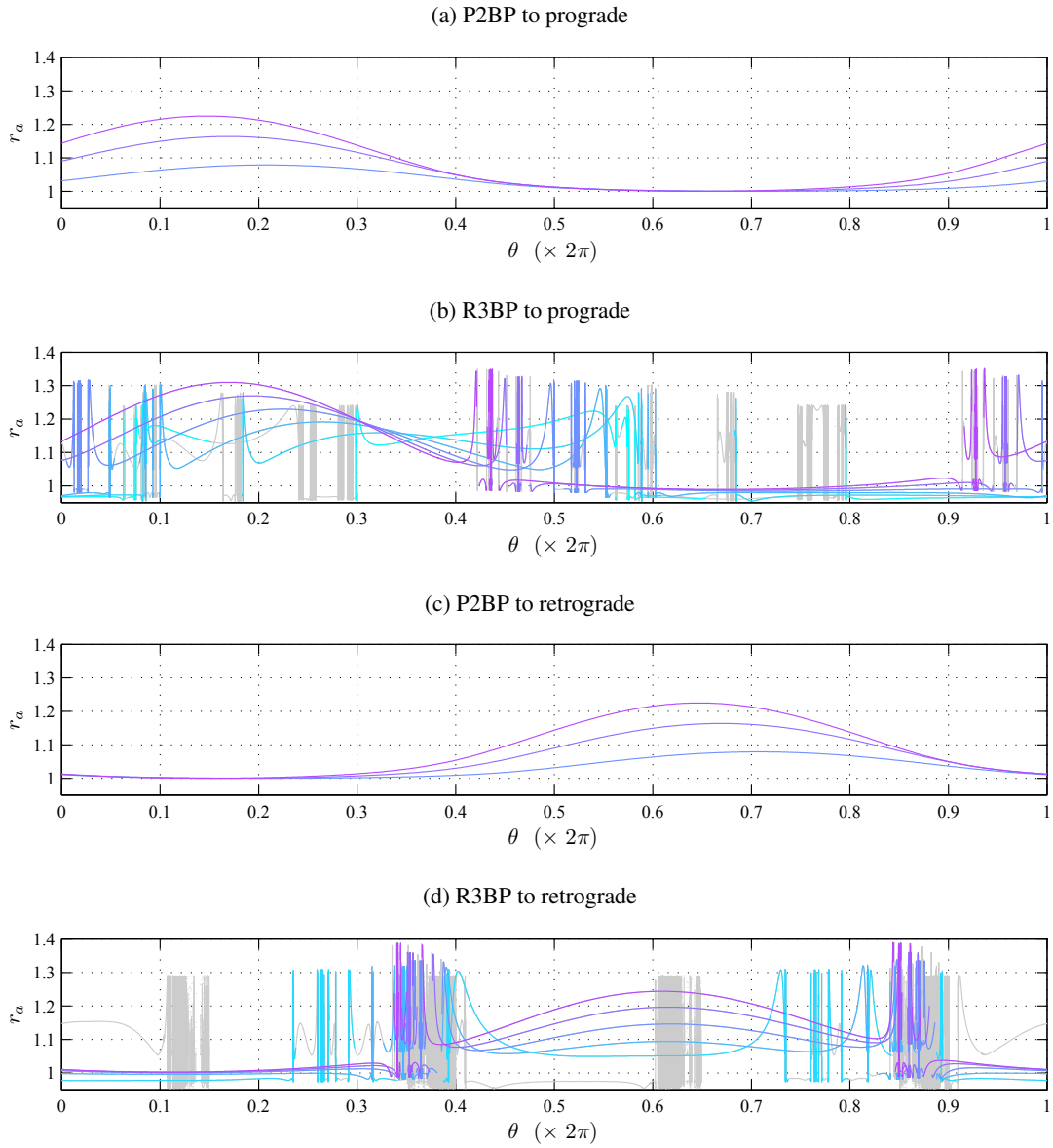

Figure 2. Apojove resulting for applying maneuver at θ; each line represents a unique Δv ranging from 0.425 (aqua) to 0.675 km/s (magenta); r_a is measured in Jupiter-Europa distances.

long duration transfers from our search. For each trajectory we store the osculating value of r_a at the end of the simulation. Simulations that reach the 500 day limit before crossing the negative X-axis are discarded, as well as if the Jacobi constant is not preserved within a prescribed tolerance.

The results of the simulations can be visualized in Figure 2 (above), where r_a is plotted in Jupiter-Europa distances. The values of Δv examined are 0.425 km/s (aqua), 0.475 km/s, 0.525 km/s, 0.575 km/s, 0.625 km/s, and 0.675 km/s (magenta). We also monitor if the trajectory passes below Europa's radius (gray). Included in Figure 2 are the curves of r_a versus θ for the P2BP for $\Delta v = 0.575$ km/s, 0.625 km/s, and 0.675 km/s. As expected, in the P2BP the curves are smooth and there is one maximum and one minimum for each Δv. The maxima occur when θ is such that the vector $\mathbf{v}_\infty$ is in the direction the Europa's motion. In the

P2BP the extremal values of r_a are the same for both prograde and retrograde orbits.

While the shape of the curves in the R3BP are similar to the P2BP, there are some striking and important differences. The most noticeable difference is the prominent spiking that occurs in Figures 2b and 2d. The spikes correspond to Europa flybys not modeled in our P2BP analysis. There is spiking as well for particular resonances in the P2BP, however, for a particular Δv, the maximum r_a achievable from those resonant encounters cannot exceed the maximum shown in Figures 2a and 2c. Alternatively, for a given Δv in the R3BP, often the spiking peaks yield much larger r_a's than the smooth peaks. For a prograde orbit, we also note that even the smooth peak in Figure 2b has a larger r_a than the peak in Figure 2a.

All the peaks in Figures 2b and 2d are stored and ordered in descending r_a. For each Δv, the top five trajectories are plotted in Figures 3 and 4, for prograde and retrograde orbits, respectively. The coordinates x, y, and z in the figures are the spacecraft's position with respect to Europa, measured in the rotating frame and units of Europa radii. The gray region is the forbidden zone as determined by the values of zero-velocity in order to satisfy Eq. (6). We also include a line corresponding to the angle at arrival θ, and the value of osculating r_a for that case is recorded in the title of each subplot. We immediately notice that the same type of transfer consistently performs well for each value of Δv. The best trajectory appears to follow an L_2 Lyapunov orbit for one revolution, where a Europa flyby then ejects the spacecraft with high r_a. In fact, for some cases the spacecraft follows the L_2 Lyapunov orbit for multiple revolutions before leaving the vicinity of Europa. The other transfers also follow well-known periodic orbits in the R3BP. (For an example of some of these orbits, see Broucke.[13]) We notice similar behavior if the orbit is retrograde. (Recall Figure 4 below.) When the orbit is retrograde, there are no capture trajectories that are not subsurface for $\Delta v = 0.425$ km/s. However, for the other Δv's the r_a values are much higher than the best prograde trajectories. Considering the similarities of the trajectories found in Figures 3 and 4, these preliminary results suggest that the approach trajectory for optimal capture is not sensitive to the orientation of the 200-km circular orbit at Europa.

Families of Transfers

In this section we come to a more satisfying dynamical understanding of the efficient trajectories found in the grid search. From Figures 3 and 4, it is not surprising that each transfer trajectory exists as a subset of a family of trajectories. To this end, we seek to compute a family of trajectories where

$$\frac{dr_a}{d\theta} = 0, \tag{10}$$

$$\frac{d^2 r_a}{d\theta^2} < 0. \tag{11}$$

A targeting scheme is derived that enforces Eq. (10). Provided the initial guess is close to the maximum, the algorithm converges to a solution that satisfies Eq. (11), as well. To formulate the targeter, first we need an expression for the derivative $dr_a/d\theta$. The derivative appears in the variation of r_a, i.e.,

$$\delta r_a = \frac{dr_a}{d\theta}\delta\theta. \tag{12}$$

From Taylor series expansion of $r_a = r_a(\mathbf{X}_f(\mathbf{X}_0(\theta), t))$ and the chain-rule,

$$\delta r_a = \frac{\partial r_a}{\partial \mathbf{X}_f}\frac{\partial \mathbf{X}_f}{\partial \mathbf{X}_0}\frac{\partial \mathbf{X}_0}{\partial \theta}\delta\theta + \frac{\partial r_a}{\partial \mathbf{X}_f}\frac{\partial \mathbf{X}_f}{\partial t}\delta t. \tag{13}$$

Note that $\mathbf{X}_f$ is the resulting six-state from integrating the initial state $\mathbf{X}_0$ backwards to the plane $Y = 0$, $X < 0$. The variation δt in Eq. (13) can be eliminated by recognizing that at the crossing $Y_f(\mathbf{X}_0(\theta), t) = 0$, so the variation is

$$\delta Y_f = \frac{\partial Y_f}{\partial \mathbf{X}_0}\frac{\partial \mathbf{X}_0}{\partial \theta}\delta\theta + \frac{\partial Y_f}{\partial t}\delta t = 0. \tag{14}$$

Solving for δt in Eq. (14) and substituting into Eq. (13) results in the expression

$$\delta r_a = \frac{\partial r_a}{\partial \mathbf{X}_f}\left[\frac{\partial \mathbf{X}_f}{\partial \mathbf{X}_0} - \frac{\dot{\mathbf{X}}_f}{\dot{Y}_f}\frac{\partial Y_f}{\partial \mathbf{X}_0}\right]\frac{\mathbf{X}_0}{\partial \theta}\delta\theta. \tag{15}$$

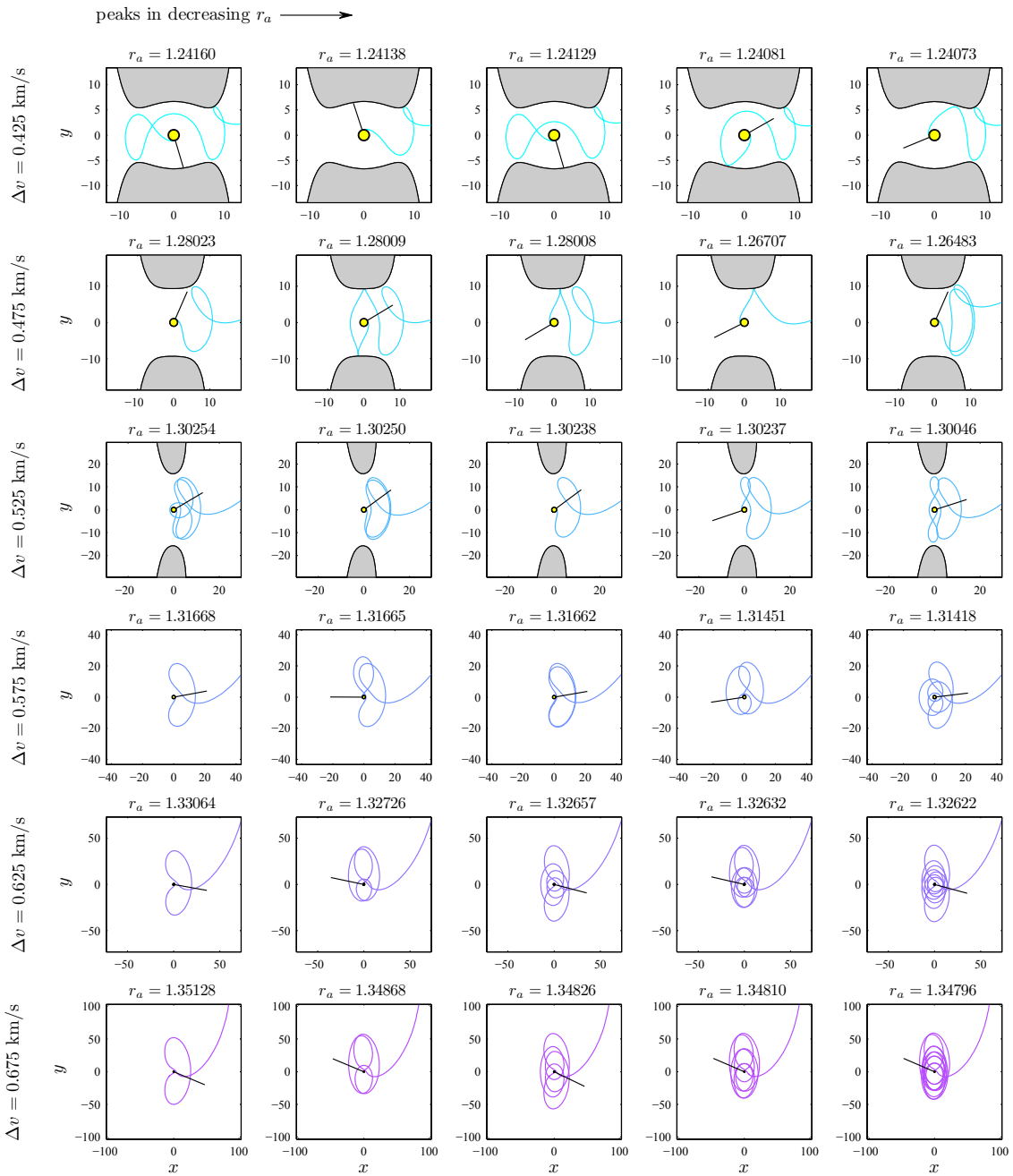

Figure 3. Top trajectories for transfer to prograde circular orbit; origin is Europa, units are Europa radii.

Hence, to satisfy Eq. (10) we desire that

$$g(\theta, \Delta v) = \frac{\partial r_a}{\partial \mathbf{X}_f} \left[\frac{\partial \mathbf{X}_f}{\partial \mathbf{X}_0} - \frac{\dot{\mathbf{X}}_f}{\dot{Y}_f} \frac{\partial Y_f}{\partial \mathbf{X}_0} \right] \frac{\mathbf{X}_0}{\partial \theta} = 0. \tag{16}$$

Initial guesses for θ and Δv are available from the grid search, and a minimum-norm Newton's method finds the precise conditions $\mathbf{Y}_j = (\theta_j, \Delta v_j)^T$ such that $g(\mathbf{Y}_j) = 0$. From $\mathbf{Y}_j$ a guess for a nearby solution in the

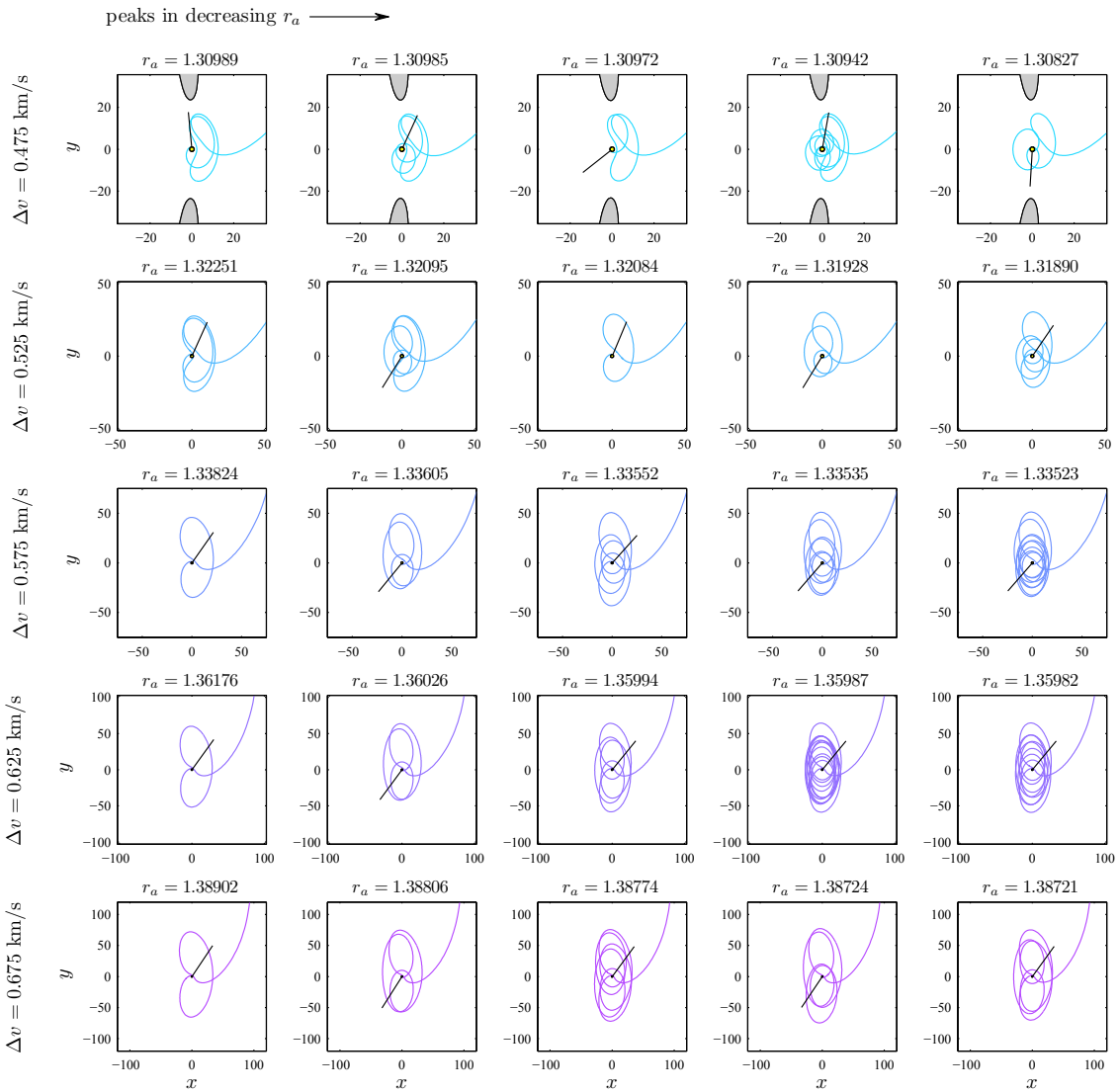

Figure 4. Top trajectories for transfer to retrograde circular orbit; origin is Europa, units are Europa radii.

family is available from

$$\mathbf{Y}_{j+1} = \mathbf{Y}_j + s\hat{\mathbf{Y}}_j, \tag{17}$$

where $\hat{\mathbf{Y}}_j$ is a unit vector in the nullspace of $Dg(\mathbf{Y}_j)$. To converge to the neighboring trajectory, the new system of equations to solve is

$$\mathbf{F}(\mathbf{Y}_{j+1}) = \left\{ \begin{array}{c} g(\mathbf{Y}_{j+1}) \\ (\mathbf{Y}_{j+1} - \mathbf{Y}_j)^T \hat{\mathbf{Y}}_j - s \end{array} \right\} = \mathbf{0}. \tag{18}$$

Note that included in $\mathbf{F}$ is the pseudo-arclength constraint enforcing that the distance between the jth and $j^{\text{th}} + 1$ solutions, projected into the nullspace of $Dg(\mathbf{Y}_j)$, is a fixed value s. The process repeats in a method of continuation, until either the peak switches from local maximum to minimum, or the trajectory at some point passes below the surface of Europa.

While continuing the family, it is important to monitor the sign of $\hat{\mathbf{Y}}_{j+1}$ to keep moving in the same direction along the family. The sign is determined such that $\hat{\mathbf{Y}}_{j+1}^T \hat{\mathbf{Y}}_j$ is always positive. For each solution, we check that the condition of maximality is satisfied, i.e., $Dg(\theta) < 0$. The scaling of the variables Δv and θ is also important. For all the families in this study, a dimensional value of Δv (km/s) is used, and for θ one revolution is set to unity. In general, the value of s in Eqs. (17) and (18) is allowed to change along the family, however, a fixed value of $s = 0.0075$ is sufficient for computing all the families in this study. This continuation method has found great success in the literature[14] and is a key component to computing various families of trajectories for efficient capture at Europa. As evidenced in Figure 2, these transfers are extremely sensitive to small changes in θ and Δv, and therefore a robust continuation scheme is critical for a successful algorithm.

For both prograde and retrograde, three families are identified corresponding to the smoother peaks in Figure 2. (See Figure 5.) The peaks outlined by these families are shown in Figure 6. When selecting peaks in Figure 2 to examine more closely, we want to be sure to take a closer look at trajectories that continually give high performance r_a in Figures 3 and 4. However, we also want to investigate the smooth peak that

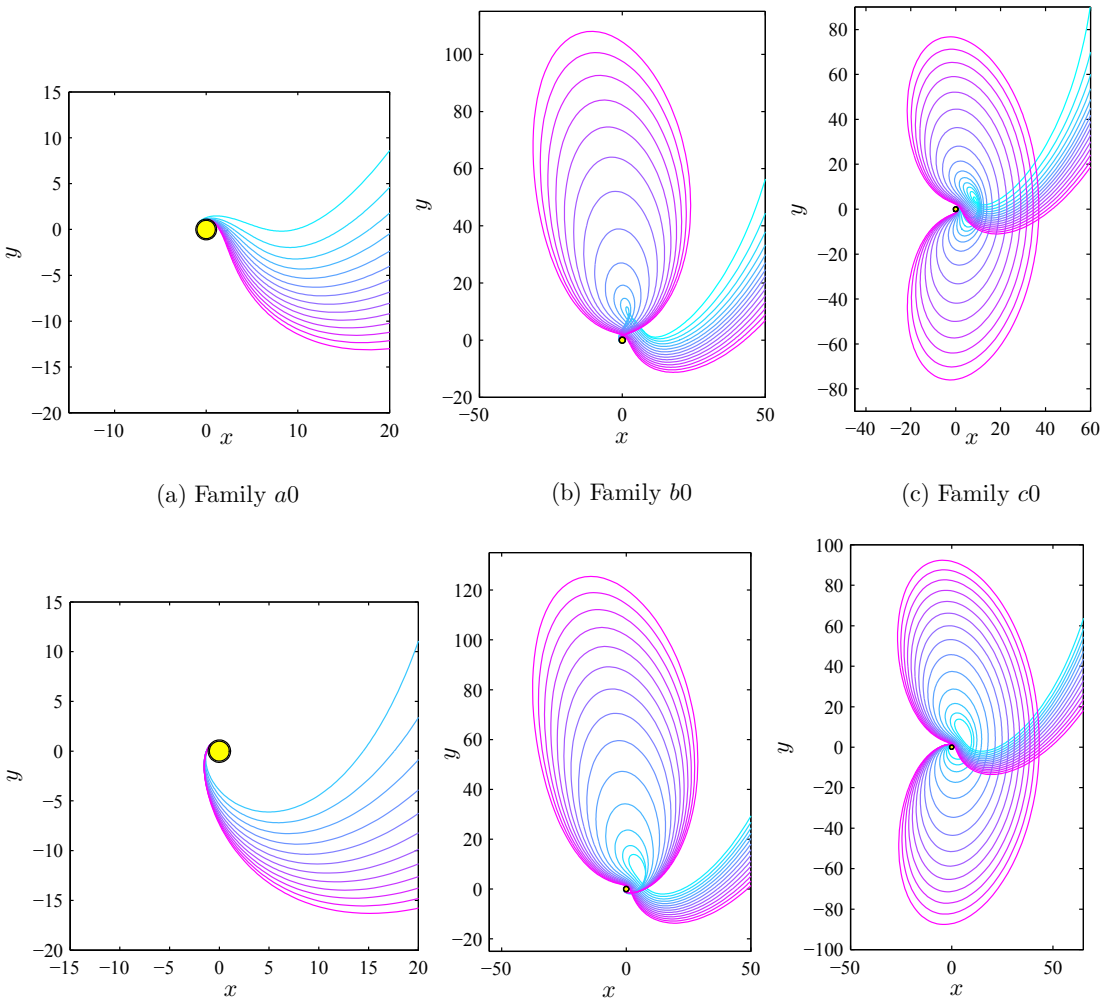

(a) Family $a0$ (b) Family $b0$ (c) Family $c0$

(d) Family $a180$ (e) Family $b180$ (f) Family $c180$

Figure 5. Various families: (a)-(c) prograde, (d)-(f) retrograde; origin is Europa, units are Europa radii

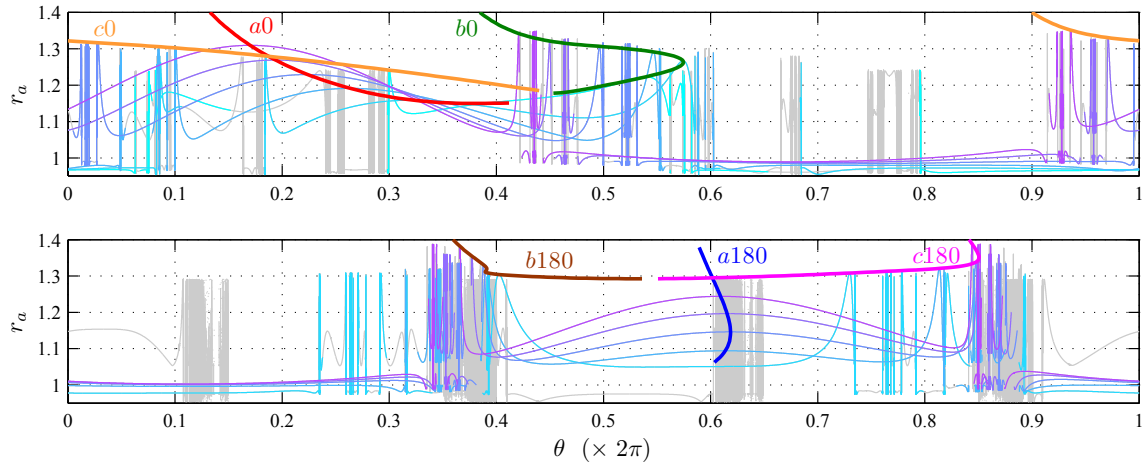

Figure 6. Line of peaks for the families.

closely resembles the one in the P2BP. Jagged peaks likely correspond to trajectories that orbit Europa many times before leaving the vicinity. While these trajectories are also fascinating, we are more interested in trajectories that quickly depart from Europa. In general, the smoother the peak in Figure 2, the faster the trajectory leaves Europa. For now, we leave the discussion of the performance of these trajectories for a later section.

TRANSFERS TO 95°-INCLINED CIRCULAR ORBITS

Investigation of planar capture trajectories is fascinating from a dynamical standpoint, yet ultimately we seek transfers to a nearly polar orbit. The currently envisioned mission calls for an orbit inclined at $95°$ to the equator. Since Europa is tidally locked, we assume the inclination can be measured with respect to the orbit plane of the primaries. When the inclination is fixed at $i = 95°$, in the P2BP there are two peaks in apojove r_a, both for values of θ and Ω that align the vector $\mathbf{v}_\infty$ with Europa's velocity. An example of when $\Delta v = 0.575$ km/s is plotted versus θ and Ω in Figure 7. The r_a-axis (z-axis) is attached to the color scale to the right of the plot. Apojove for the two peaks is roughly equal to 1.08 times the distance between Jupiter and Europa.

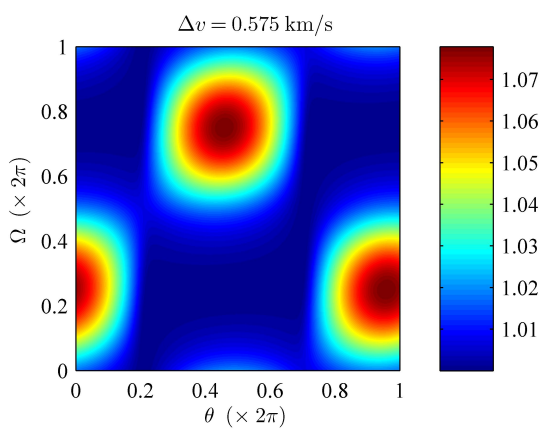

Figure 7. Apojove for all possible θ and Ω in the P2BP, $i = 95°$.

Similar to the study of planar trajectories, a grid search is performed for 3-dimensional transfer trajectories in the R3BP. Once again, trajectories are integrated for each value of Δv, and osculating values of r_a are recorded when the trajectory first crosses the plane $Y = 0$, $X < 0$. The initial states correspond to all combinations of 1,000 linearly equally spaced points for θ and Ω ranging from $0°$ to $360°$. The results of the grid search are plotted in Figure 8. Due to symmetries about the X-Y plane in the R3BP, the plots in Figure 8 also possesses symmetry. For initial conditions in the white region, either the Jacobi constant is not preserved to sufficient accuracy, or the trajectories fail to leave Europa after 500 days. Recall that the gray region corresponds to trajectories that pass below Europa's surface. For larger Δv's, there are two subtle peaks and valleys, similar to the P2BP example in Figure 7. The prominent spiking between those peaks and valleys is associated with trajectories that re-encounter Europa before leaving. For the values of Δv sampled,

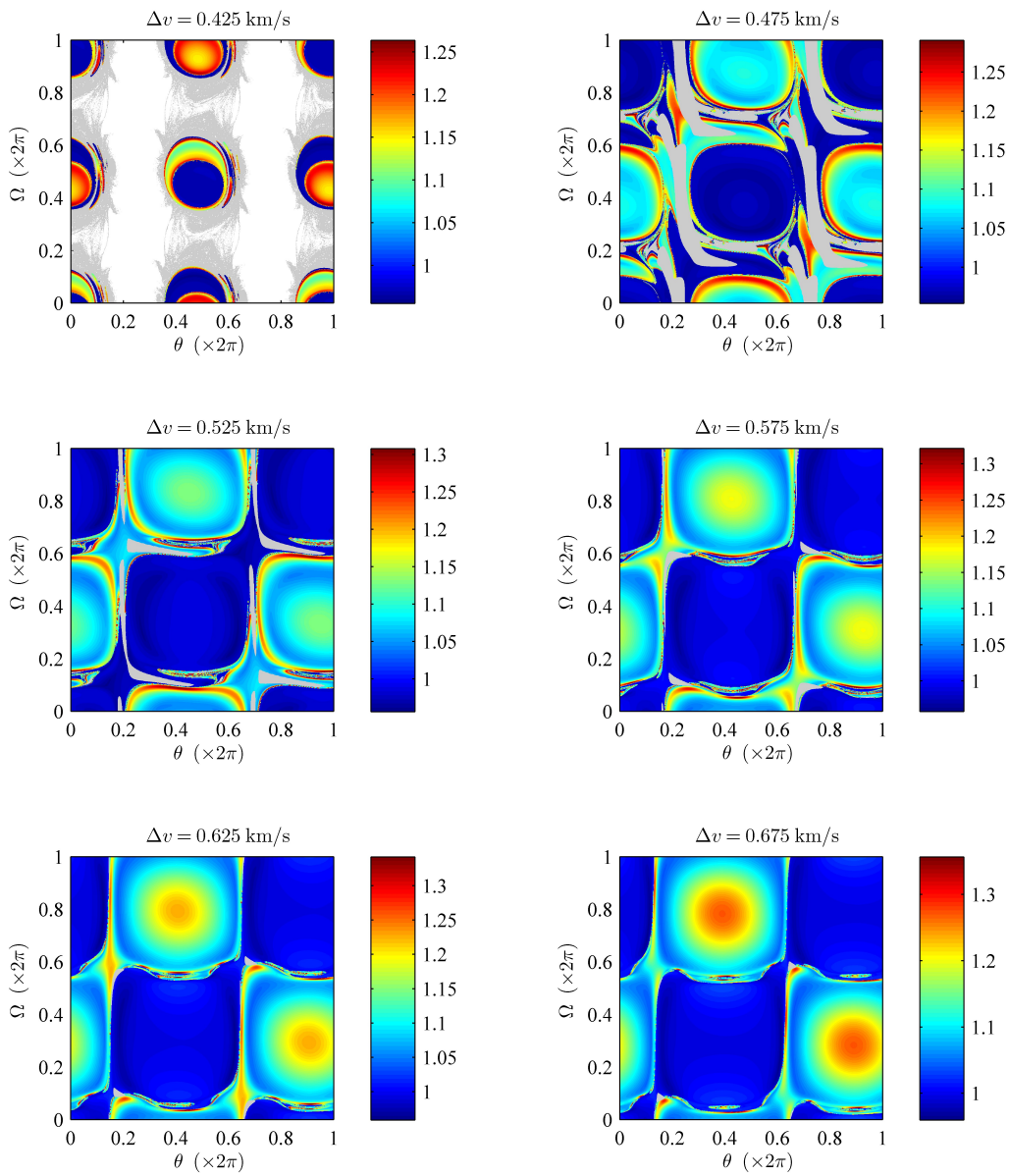

Figure 8. R3BP apojove resulting for applying maneuver at θ and Ω, $i = 95°$; the colorbar to the right indicates the value of r_a in Jupiter-Europa distances.

the darkest red always occurs in these special regions. We note also that the highest peak for $\Delta v = 0.575$ km/s is about $r_a = 1.32$, a value much higher than the P2BP maximum of 1.08 (recall Figure 7). The top five trajectories for each Δv are plotted in Figure 9. As expected due to the symmetries in the R3BP, the trajectories shown in Figure 9 occur in pairs. The shapes of the top performing trajectories for $i = 95°$ are similar to the best trajectories from $i = 0°$ and $180°$. The performance of the trajectories that yield the highest r_a is between that of $i = 0°$ and $180°$, with $i = 180°$ giving the best results. (For example, compare the r_a's recorded in each row of Figures 3, 4, and 9.)

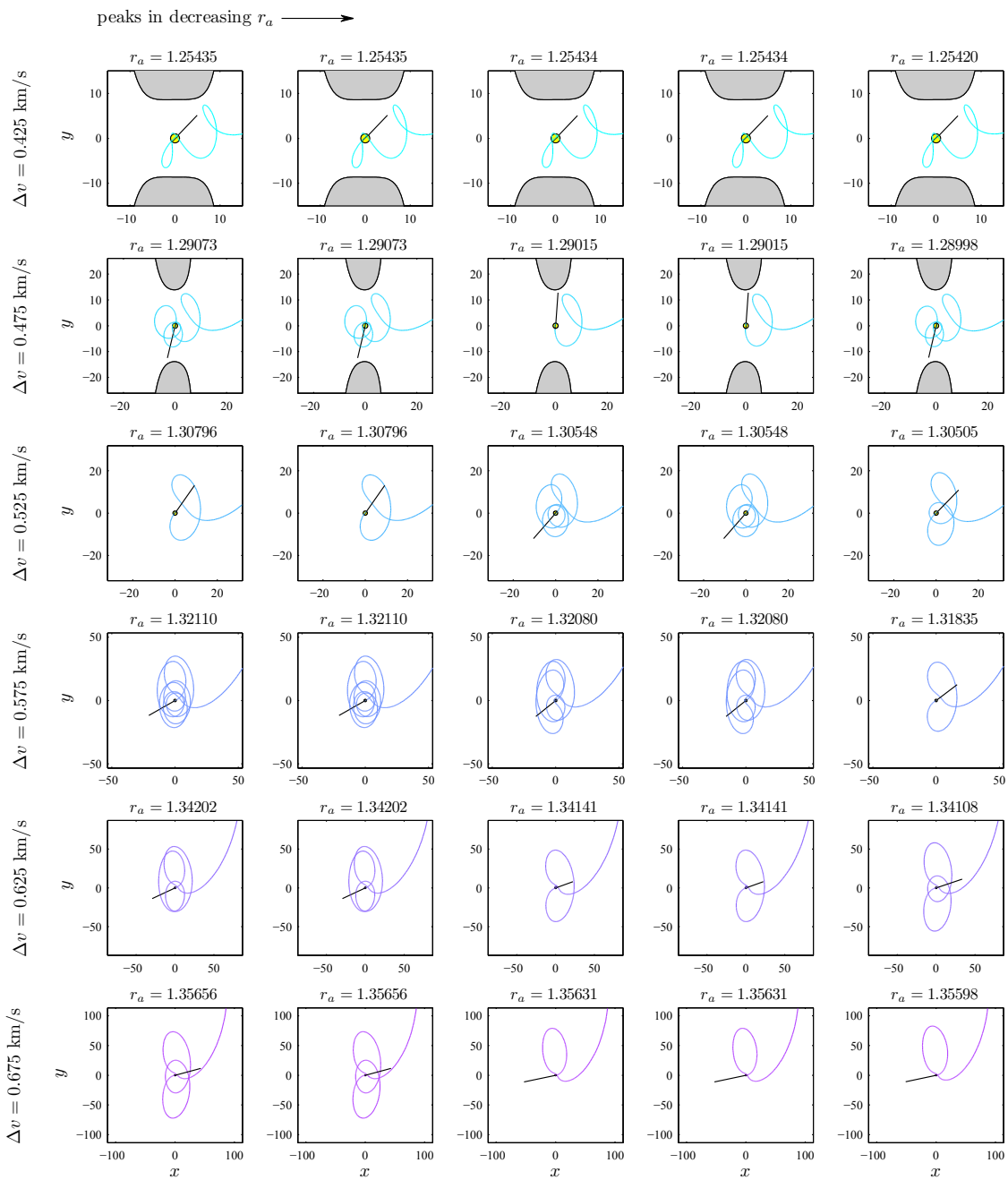

Figure 9. Top transfers to circular orbit where $i = 95°$; origin is Europa, units are Europa radii.

As with the planar transfers, transfers to circular orbits inclined at $i = 95°$ are characterized as members of families. Each peak in Figure 8 serves as an initial guess for an algorithm that adjusts θ, Ω and Δv until

$$\frac{dr_a}{d\theta} = 0 \text{ and } \frac{dr_a}{d\Omega} = 0. \tag{19}$$

These conditions are equivalent to the vector constraint

$$\mathbf{g}(\theta, \Omega, \Delta v) = \left\{ \begin{array}{c} \dfrac{\partial r_a}{\partial \mathbf{X}_f} \left[\dfrac{\partial \mathbf{X}_f}{\partial \mathbf{X}_0} - \dfrac{\dot{\mathbf{X}}_f}{\dot{Y}_f} \dfrac{\partial Y_f}{\partial \mathbf{X}_0} \right] \dfrac{\mathbf{X}_0}{\partial \theta} \\ \dfrac{\partial r_a}{\partial \mathbf{X}_f} \left[\dfrac{\partial \mathbf{X}_f}{\partial \mathbf{X}_0} - \dfrac{\dot{\mathbf{X}}_f}{\dot{Y}_f} \dfrac{\partial Y_f}{\partial \mathbf{X}_0} \right] \dfrac{\mathbf{X}_0}{\partial \Omega} \end{array} \right\} = \mathbf{0}. \tag{20}$$

Once Eq. (20) is satisfied, Eq. (17) makes a prediction for a nearby transfer in the same family, where now $\mathbf{Y}_j = (\theta_j, \Omega_j, \Delta v_j)^T$, and $\hat{\mathbf{Y}}_j$ is a unit vector in the nullspace of $D\mathbf{g}(\mathbf{Y}_j)$. The equations for continuation are Eq. (18), and g is replaced by the vector constraint $\mathbf{g}$ in Eq. (20). As the continuation progresses, it is important to monitor the eigenvalues of $D\mathbf{g}(\theta, \Omega)$ to ensure that solution corresponds to a local maximum.

The families examined for $i = 95°$ are plotted in Figure 10. From Figure 10c, it appears that the c-type

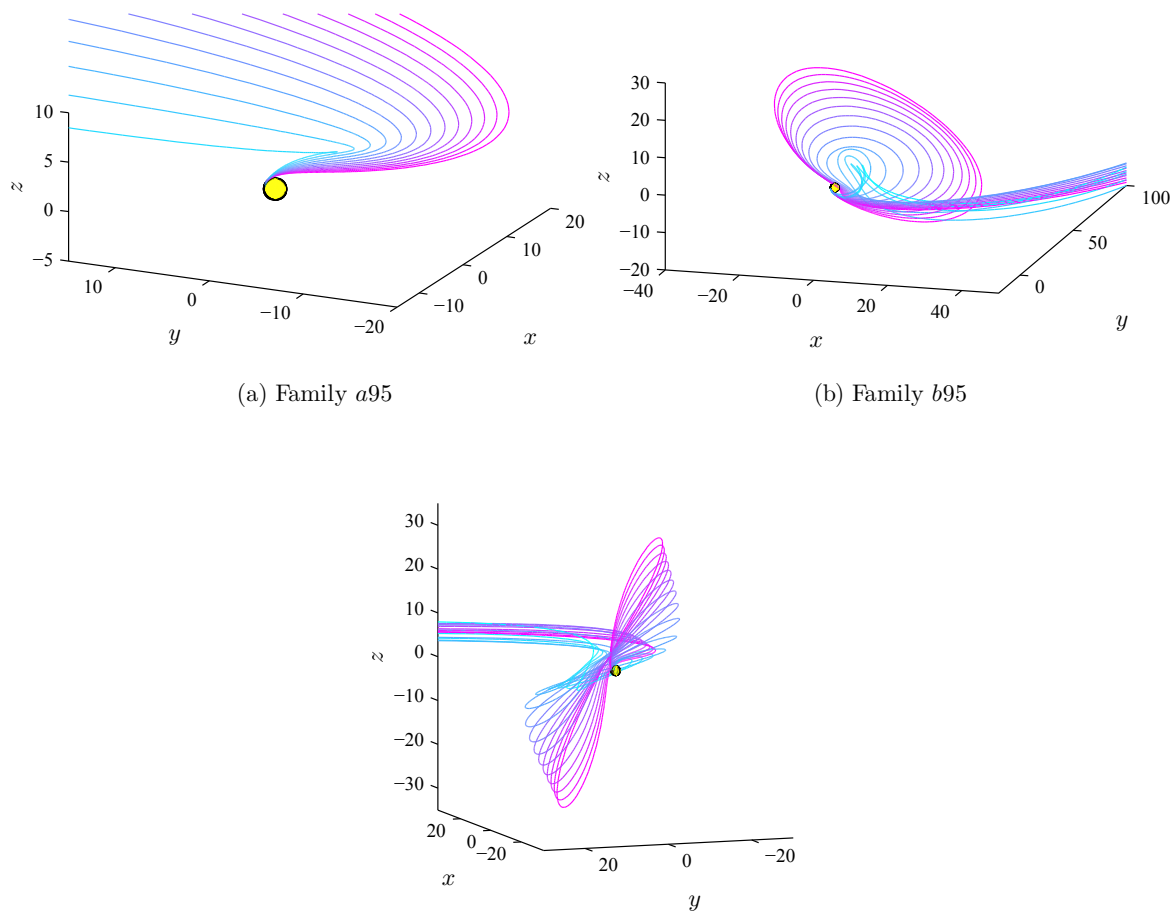

(a) Family $a95$

(b) Family $b95$

(c) Family $c95$

Figure 10. Various families for $i = 95°$; origin is Europa, units are Europa radii.

family is following either an L_2 axial orbit before insertion, or the invariant manifolds of an L_2 vertical orbit. (For examples of vertical and axial orbits, see Doedel et al.[14]). While these families are more thoroughly discussed in the following section, for now we briefly mention that the a-, b-, and c-type trajectories appear to exist for all values of i.

ANALYSIS OF RESULTS

The results for the families are discussed and an algorithm is presented for attaching efficient capture trajectories to a baseline mission. Two different capture options are proposed for the current JEO mission architecture.

Comparison of Families

We are now in a position to compare the r_a performance of the a-, b-, and c-type trajectories. In Figure 11, r_a is plotted as a function of Δv for the trajectories in each family. Also included in the plot is the r_a achieved in the P2BP for values above the Δv required for parabolic capture. While the minimum theoretical Δv for capture from $r_a = 1$ is 556 m/s, in the R3BP there are Δv's as low as 402 m/s that originate from $r_a = 1.19$. These trajectories are part of the $c0$ family (orange). For only 50 m/s more, the $c180$ family (magenta) includes a transfer from $r_a = 1.3$. We note that while all the R3BP families yield better results than the P2BP, the b- and c-type trajectories consistently outperform the a-type trajectories. An interesting

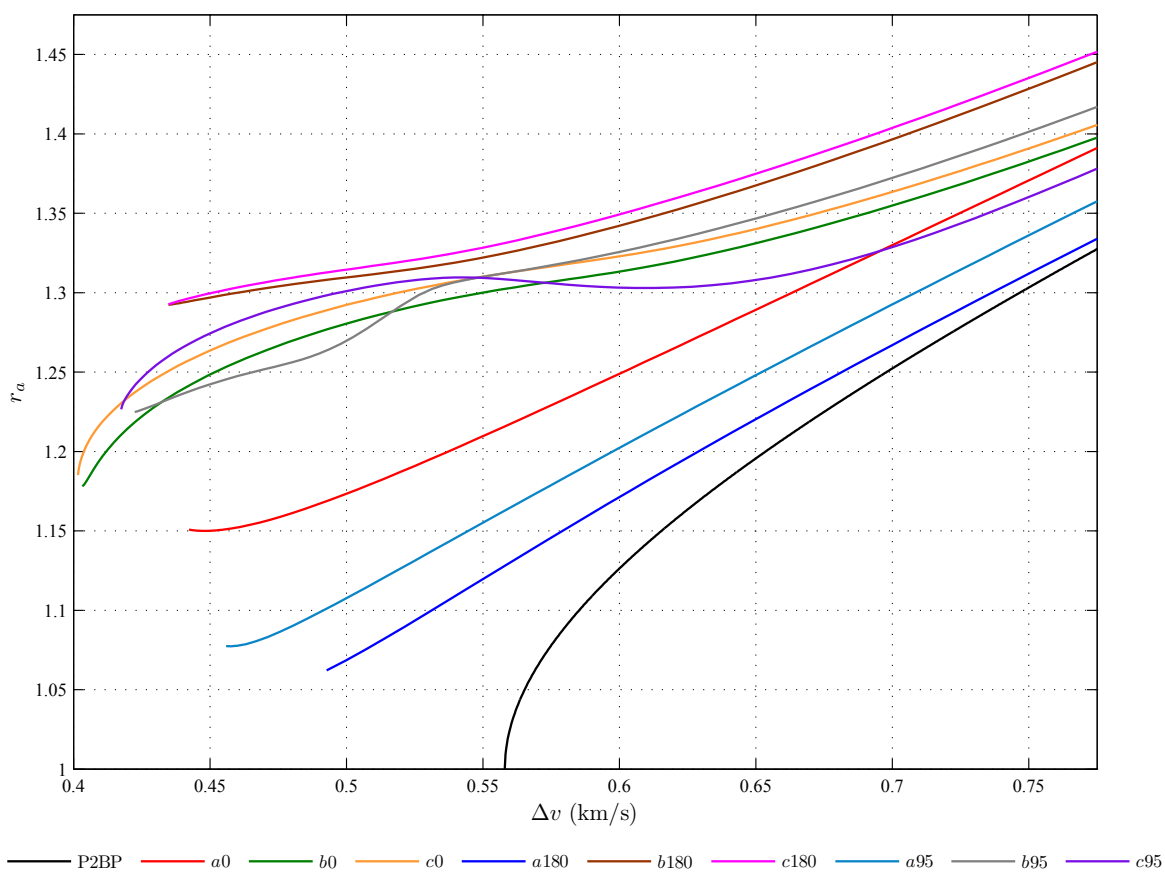

Figure 11. r_a versus Δv for each family.

trade occurs at $\Delta v = 550$ m/s between the $b95$ (gray) and $c95$ (purple) families. Below $\Delta v = 550$ m/s, the $c95$ family includes trajectories from higher r_a's, whereas above 550 m/s the $b95$ family gives the higher r_a's. In fact, for the $c95$ family, r_a briefly decreases following 550 m/s.

To measure the performance of the trajectories, consider the minimum Δv, single burn strategy necessary to transfer from r_a in the P2BP. Assuming the spacecraft is already on the inbound trajectory from r_a, the minimum Δv corresponds to insertion from a Hohmann transfer arc. The Δv at insertion is

$$\Delta v_{P2BP} = \sqrt{\left(\sqrt{\frac{2r_a(1-\mu)}{1+r_a}} - \sqrt{1-\mu}\right)^2 + \frac{2\mu}{r_c} - \sqrt{\frac{\mu}{r_c}}}. \tag{21}$$

Then, the fractional savings in Δv using a multi-body transfer from the same r_a is

$$\eta = \frac{\Delta v_{P2BP} - \Delta v_{R3BP}}{\Delta v_{P2BP}}. \tag{22}$$

We compute η for the a-, b-, and c-type trajectories, and the results are plotted in Figure 12. To appreciate the importance of these results, compare a multi-body transfer from $r_a = 1.3$ to the equivalent minimum-energy Hohmann transfer. Ignoring the Δv at apojove and assuming the spacecraft is already on the inbound transfer from $r_a = 1.3$, the Hohmann transfer Δv for insertion is about 750 m/s. For an alternative single

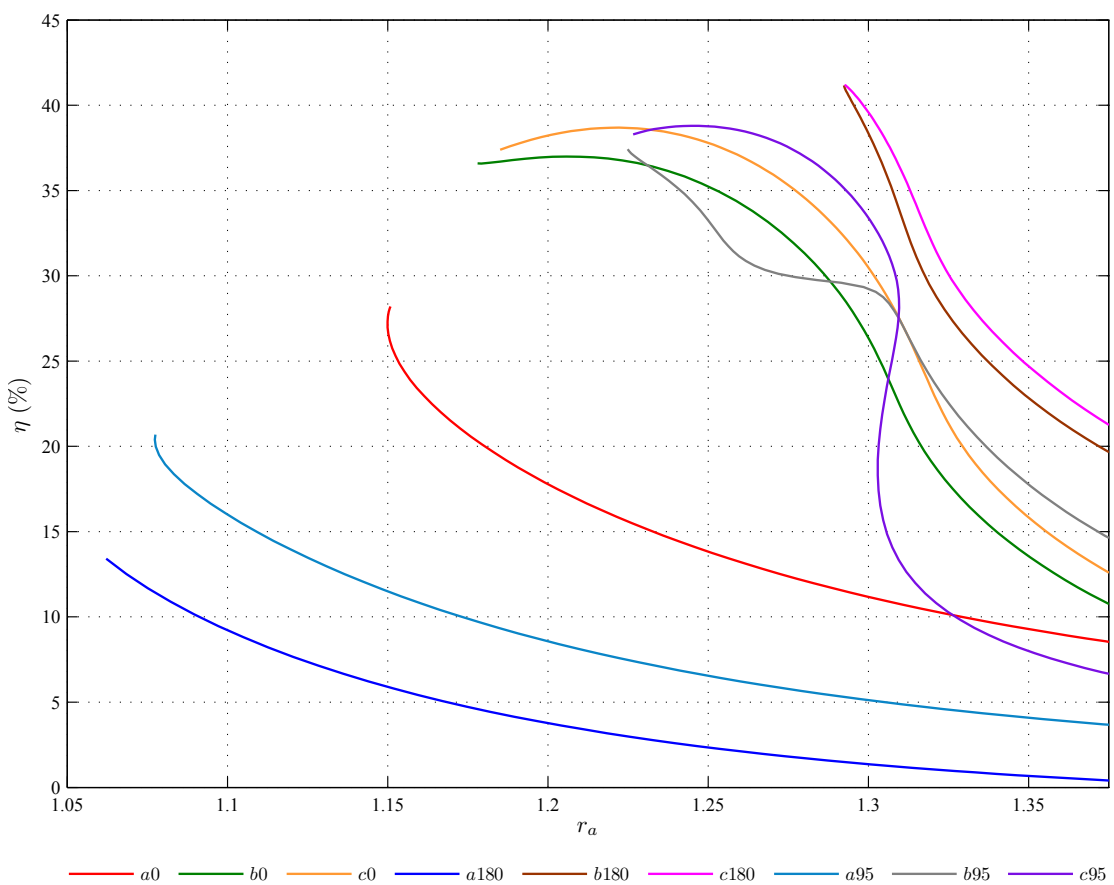

Figure 12. Percent savings in Δv for transfer from r_a.

burn strategy, from Figure 12 we see there is a transfer trajectory in the $c180$ family that saves 40% of this Δv. The trajectory achieves the same objective for 300 m/s less.

Mission Oriented Examples

Attaching a multi-body trajectory to the baseline mission is a critical step in verifying the usefulness of these trajectories for mission design. Here we demonstrate that it is not essential to start with an a-, b-, and c-type trajectory that perfectly matches the spacecraft-Jupiter-Europa phasing of a nominal mission.

The envisioned baseline for JEO is the tour T08-008 presented in Kloster et al.[5] The final phase of the tour before insertion is depicted in Figure 13. The last flyby before capture is the E24 flyby on June 12, 2028, where the incoming $v_\infty^- = 1.17$ km/s. Since we desire a ballistic flyby, the magnitude of the post flyby vector $\mathbf{v}_\infty^+$ must also equal 1.17 km/s, however, in general the direction is allowed to vary. Assuming the position of the spacecraft coincides with Europa, Eqs. (1) are then integrated with $\mu = 0$ to successive apojoves $\mathbf{R}_{r_a}^-$. At capture, we note that for each multi-body family of trajectories, θ and Ω are functions of the insertion Δv. Guessing a reasonable Δv, we interpolate the values of θ and Ω from the family data and integrate backwards to successive apojoves $\mathbf{R}_{r_a}^+$. For the backwards integration, μ is the actual Jupiter-Europa mass ratio. The number of apojoves selected depends on both the resonance of the trajectory and which apoapsis is selected for the match point. For our study, we investigated the effects of placing the match point at all possible apoapses. A velocity discontinuity, or Δv_{r_a}, is allowed at the match point. This velocity

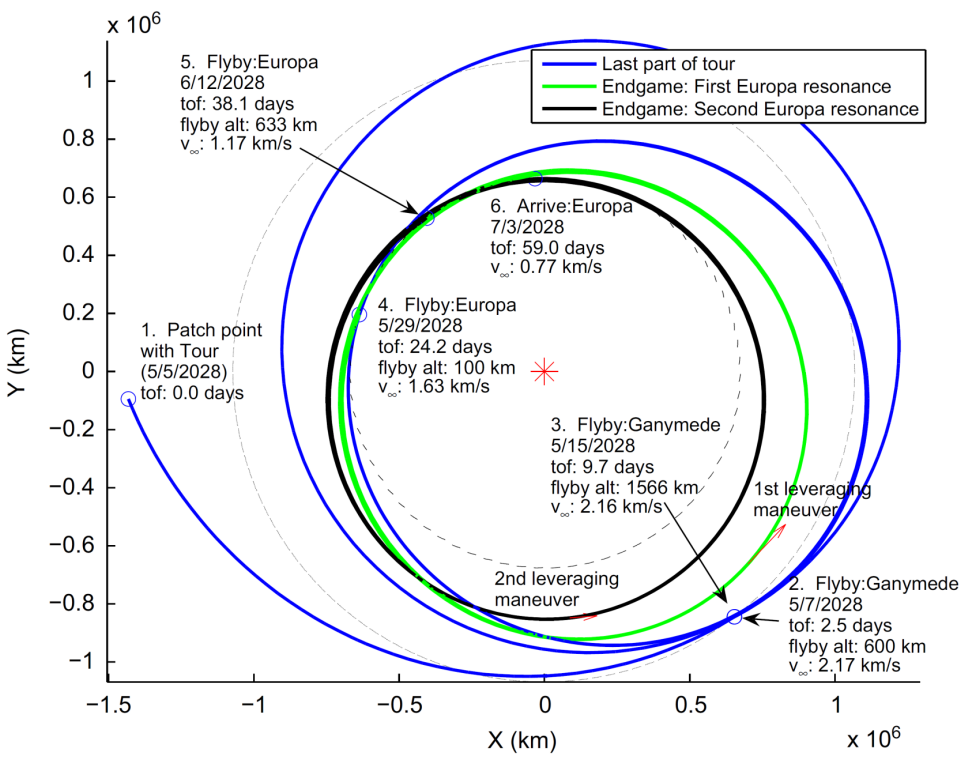

Figure 13. Courtship phase for tour T08-008.[5]

discontinuity represents a maneuver at apojove. In brief, the variables of the algorithm are

$$\mathbf{Y} = \left\{ \begin{array}{c} \mathbf{v}_\infty^+ \\ \Delta v \end{array} \right\}, \tag{23}$$

where the constraints to satisfy are

$$\mathbf{F}(\mathbf{Y}) = \left\{ \begin{array}{c} ||\mathbf{v}_\infty^+|| - ||\mathbf{v}_\infty^-|| \\ \mathbf{R}_{r_a}^+ - \mathbf{R}_{r_a}^- \end{array} \right\} = \mathbf{0}. \tag{24}$$

In Eq. (24), both $\mathbf{R}_{r_a}^+$ and $\mathbf{R}_{r_a}^-$ are measured with respect to the Jupiter-Europa barycenter. Guessing a reasonable $\mathbf{Y}$, a Newton's method satisfies the constraint Eqs. (24). Once a solution is found, it is important to check the angle between $\mathbf{v}_\infty^+$ and $\mathbf{v}_\infty^-$ to ensure that the altitude of the flyby is acceptable.

The algorithm successfully attaches a trajectory from the $c95$ family to the end of the T08-008 tour. Post E24 flyby, the trajectory is plotted in Figure 14. As in Figure 13, the time of flight is measured in days past May 5, 2028. The trajectory requires 19 more days than the T08-008 tour. Kloster et al. report a maneuver between E24 and EOI at 66 m/s. The Δv_{mp} for the trajectory shown in Figure 14 is 153 m/s. Whereas the insertion Δv for the T08-008 tour is 707 m/s, the $c95$-type trajectory only requires 436 m/s. The total savings is 118 m/s. This is a significant savings representing roughly 15% of the entire Δv allotted for the Jovian tour.

As an alternative, insertion following the E23 flyby is perhaps a better strategy. The E24 flyby puts the spacecraft in a 6:5 resonance with Europa with low apoapses that might be costly in terms of radiation dose. We can discard the 6:5 resonance and capture following the 4:3 resonance by using a $b95$-type trajectory. The post E23 trajectory is shown in Figure 15. Here $\Delta v_{r_a} = 99$ m/s and performed at the first apoapsis following E23. Europa orbit insertion is 4.3 days earlier than the T08-008 tour, and the total Δv required is only 27 m/s more than the nominal T08-008 tour.

We want to stress that the Δv_{r_a} is non-optimal with this method. These options for capture serve as initial guesses for an optimizer that further reduces the total Δv in a full ephemeris model and with fully integrated propagation. We speculate that the total cost can be lowered perhaps by 50 m/s more via optimization.

CONCLUSION

Millions of trajectories for capture at EOI are investigated. Prograde and retrograde orbits are considered, as well as a 200-km circular orbit inclined at $95°$ to the Jupiter-Europa plane. An algorithm is presented for computing the trajectories as members of a family of transfers, and three new types of transfer are identified. The trajectories are evaluated in terms apojove performance. The top performing trajectories appear to follow L_2 Lyapunov orbit invariant manifolds leading to capture to a retrograde orbit, and in some cases saving up to 40% of Δv from the P2BP. A method is developed for patching the trajectories into a baseline tour, and two capture trajectories are proposed for the current JEO baseline mission. While the first option saves over 100 m/s in Δv, the second option might be more useful in that insertion occurs following the 4:3 resonance and without a significant penalty in Δv.

This solution approach for identifying capture trajectories can easily be adapted for a study of escape trajectories. Due to the symmetries in the R3BP, the apojove performance for the escape trajectories is equivalent to that for capture. Furthermore, the method is not dependent on a specific inclination, nor does it require the circular orbit be at 200-km altitude. An interesting application for this approach might be the investigation of transfers to low-altitude lunar orbits that originate from the smallest possible perigee.

Future work includes exploring unstable periodic orbits as waypoints to Europa. Adapting the method proposed by Koon et al.,[6] the keys to an even better understanding of the results presented in this work may involve the study of invariant manifolds of periodic orbits nearby Europa.

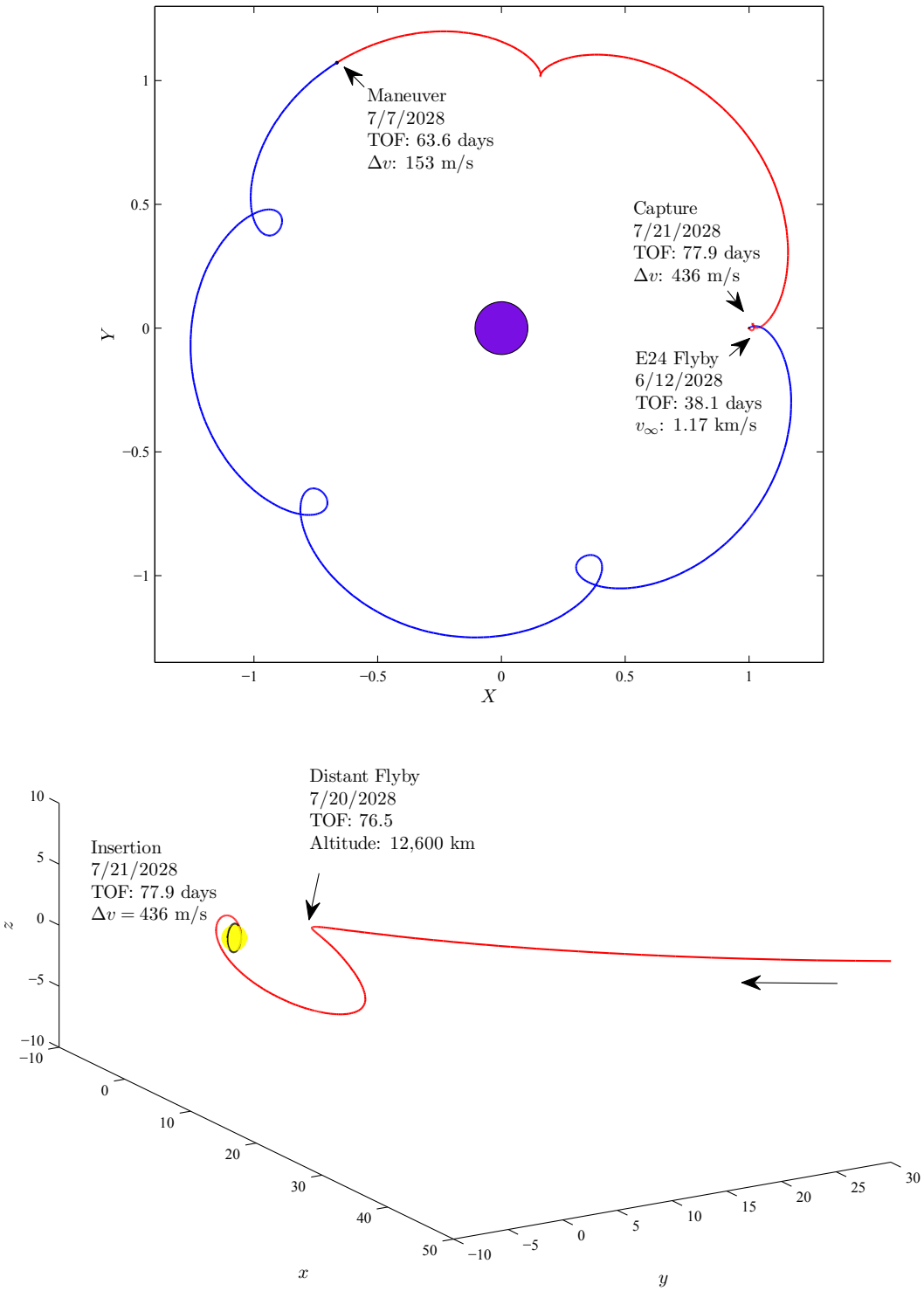

Figure 14. Attaching a $c95$-type trajectory at E24 of the T08-008 tour; rotating, barycentric, Jupiter-Europa coordinates (top), and rotating, Europa centered, coordinates in Europa radii (bottom).

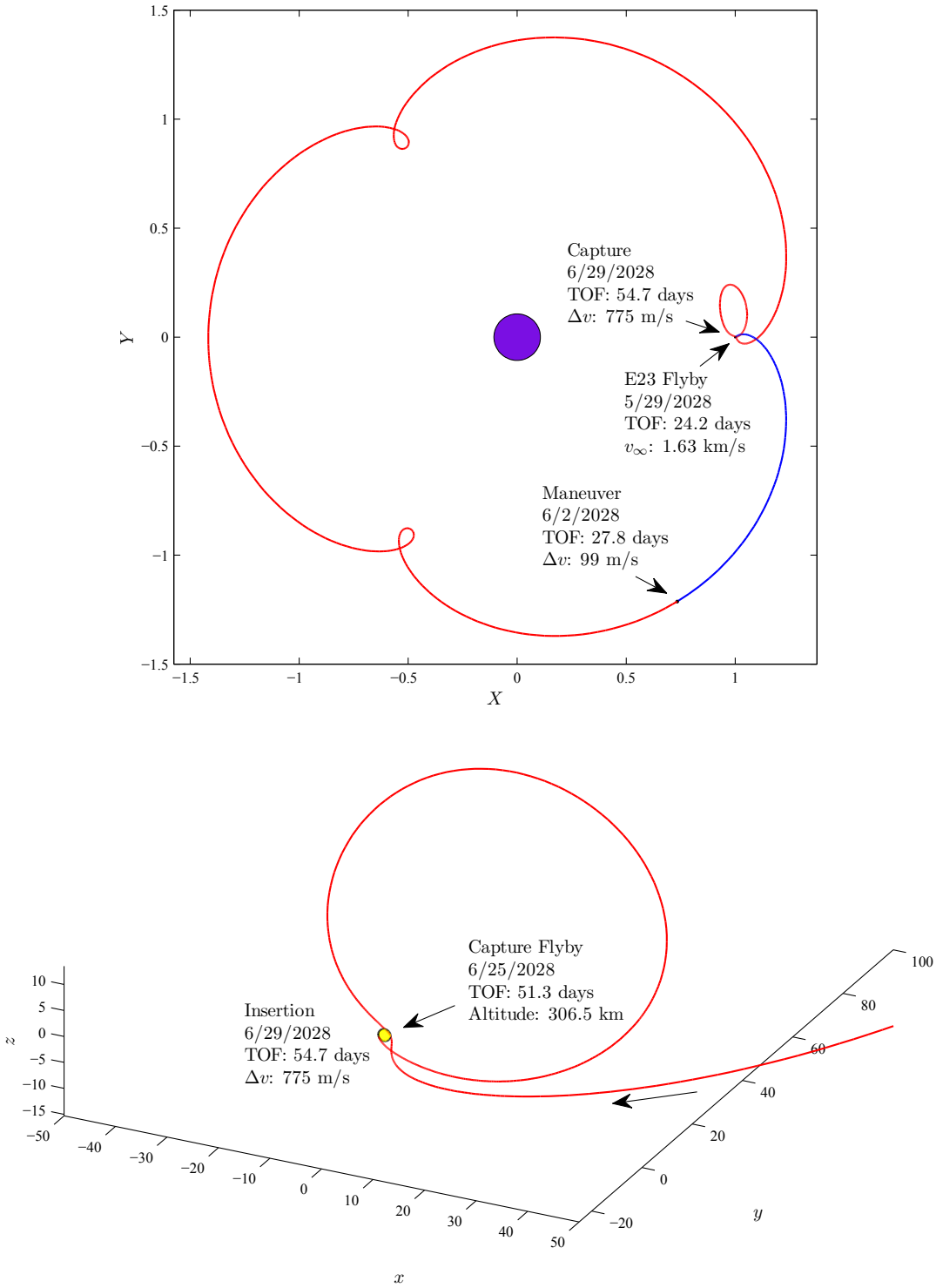

Figure 15. Attaching a $b95$-type trajectory at E23 of the T08-008 tour; rotating, barycentric, Jupiter-Europa coordinates (top), and rotating, Europa centered, coordinates in Europa radii (bottom).

ACKNOWLEDGMENT

This research was carried out at the Jet Propulsion Laboratory, California Institute of Technology, under a contract with the National Aeronautics and Space Administration. The authors thank Stefano Campagnola, Jon Sims, and Chen-Wan Yen for their insights provided for this work.

REFERENCES

[1] "Europa Jupiter System Mission: A Joint Endeavor by ESA and NASA," *Europa Jupiter System Mission Joint Summary Report*, National Aeronautics Space Administration and The European Space Agency, January 16, 2009.

[2] T. Sweetser, R. Maddock, J. Johannesen, J. Bell, P. Penzo, A. Wolf, S. Williams, S. Matousek, and S. Weinstein, "Trajectory design for a Europa Orbiter mission: a plethora of astrodynamics challenges," AAS Paper No. 97-174, *AAS/AIAA Space Flight Mechanics Meeting*, Huntsville, Alabama, February 10-12, 1997.

[3] J. Johannesen and L. D'Amario, "Europa orbit mission trajectory design," AAS Paper No. 99-360, *AAS/AIAA Astrodynamics Specialists Conference*, Girdwood, Alaska, August 15-19, 1999.

[4] M. Khan, S. Campagnola, and M. Croon, "End-to-End mission analysis for a low-cost, two spacecraft mission to Europa," AAS Paper No. 04-132, *AAS/AIAA Space Flight Mechanics Meeting*, Maui, Hawaii, February 8-12, 2004.

[5] K. Kloster, A. Petropoulos, and J. Longuski, "Europa Orbiter tour design with Io gravity assists", *Acta Astronautica*, Vol. 68, No. 7-8, 2011, pp. 931-946.

[6] W. Koon, M. Lo, J. Marsden, and S. Ross, "Constructing a Low Energy Transfer Between Jovian Moons," *Contemporary Mathematics*, Vol. 292, 2002, pp. 129-146.

[7] S. Campagnola and R. Russell, "The Endgame Problem Part A: V-Infinity Leveraging Technique and the Leveraging Graph," AAS Paper No. 09-224, *AAS/AIAA Space Flight Mechanics Meeting*, Savannah, Georgia, February 8-12, 2009.

[8] S. Campagnola and R. Russell, "The Endgame Problem Part B: The Multi-Body Technique and the T-P Graph," AAS Paper No. 09-227, *AAS/AIAA Space Flight Mechanics Meeting*, Savannah, Georgia, February 8-12, 2009.

[9] V. Szebehely, *Theory of Orbits: The Restricted Problem of Three Bodies*. New York: Academic Press, 1967.

[10] T. Sweetser, "Jacobi's Integral and ΔV-Earth-Gravity-Assist (ΔV-EGA) Trajectories," AAS Paper No. 93-635, *AAS/AIAA Astrodynamics Specialist Conference*, Victoria, British Columbia, Canada, August 16-19, 1993.

[11] C. Conley, "Low Energy Transit Orbits in the Restricted Three-Body Problem," *SIAM Journal of Applied Mathematics*, Vol. 16, No. 4, 1968.

[12] L. Shampine and H. Watts, *DEPACK-Design of a User Oriented Package of ODE Solvers.* SAND79-2374, Sandia National Laboratories, Albuquerque, New Mexico, 1980.

[13] R. Broucke, "Periodic Orbits in the Restricted Three-Body Problem with Earth-Moon Masses," NASA Technical Report 32-1168, Jet Propulsion Laboratory, Pasadena, CA, 1968.

[14] E. Doedel, V. Romanov, V. Paffenroth, H. Keller, D. Dichmann, J. Galán-Vioque, and A. Vanderbauwhede, "Elemental Periodic Orbits Associated with the Libration Points in the Circular Restricted 3-Body Problem," *International Journal of Bifurcation and Chaos*, Vol. 17, No. 8, pp. 2625-2677, 2007.